EGYPTIAN JOURNAL OF BOTANY (EJBO)

Print ISSN: 0375-9237
Online ISSN: 2357-0350

Anti-candidal activity of mycosynthesized silver nanoparticles using novel rhizosphere soil fungus from Saudi Arabia

Fatimah A. Alqahtani, Enas M. Ali, Basem M. Abdallah

PUBLISHED BY
THE EGYPTIAN
BOTANICAL SOCIETY

Anti-candidal activity of mycosynthesized silver nanoparticles using novel rhizosphere soil fungus from Saudi Arabia

Fatimah A. Alqahtani[1], Enas M. Ali[1,2], Basem M. Abdallah[1]

[1]Department of Biological Sciences, College of Science, King Faisal University, Al-Ahsa, 31982, Saudi Arabia
[2]Department of Botany and Microbiology, Faculty of Science, Cairo University, Cairo, Egypt

Candida albicans is considered as an opportunistic yeast fungus that is considered as the principal reason of dangerous invasive infections with high death rates. In this research, we were the first to mycosynthesize silver nanoparticles (AgNPs) from the rhizospheric fungus *Penicillium griseofulvum* (PG) cell-free filtrate (CFF) and examined their antifungal effectiveness alone or in combination with the antifungal Amphotericin B (PG-AgNPs/AMB) against *C. albicans*. A total of 155 fungal isolates, which were recovered from the rhizosphere soil of *Reseda pentagyna*, belonged to fifteen species represented by five different genera. PG-AgNPs were characterized by transmission electron microscopy (TEM), energy dispersive X-ray analysis (EDX), zeta potential, X-ray diffraction (XRD), UV-Vis spectroscopy, and Fourier transform infrared spectroscopy (FTIR). The disc diffusion assay presented the anti-candidal activity of PG-AgNPs against *C. albicans* with a minimum inhibitory concentration (MIC) of 16 µg/mL. Additionally, PG-AgNPs/AMB (16/32 µg/mL) exhibited a potent synergistic antifungal activity with an inhibition zone of 27 mm. PG-AgNPs/AMB (16/32 µg/mL) completely inhibited morphogenesis and repressed the adherence and biofilm establishment of *C. albicans* by 91% and 87%, respectively. Interestingly, PG-AgNPs/AMB suppressed the antioxidant-related enzymes in *C. albicans* by more than 80%. PG-AgNPs/AMB displayed cytoplasm degeneration and damage of cell wall as examined by scanning and transmission electron microscopy. Remarkably, PG-AgNPs did not show any signs of cytotoxicity on either primary mesenchymal stem cells or human gingival fibroblast cell line HGF-1. In conclusion, we identified PG-AgNPs/AMB as an innovative therapeutic candidate for the treatment of candidiasis.

Key words: Silver nanoparticles; *Candida albicans*; *Penicillium griseofulvum*; candidiasis

ARTICLE HISTORY
Submitted: October 20, 2024
Accepted: November 21, 2024

CORRESPONDANCE TO
Basem M. Abdallah,
Department of Biological Sciences,
College of Science, King Faisal University,
Al-Ahsa, 31982, Saudi Arabia
Email: babdallallah@kfu.edu.sa
DOI: 10.21608/ejbo.2024.329114.3039

EDITED BY: N. Khalil

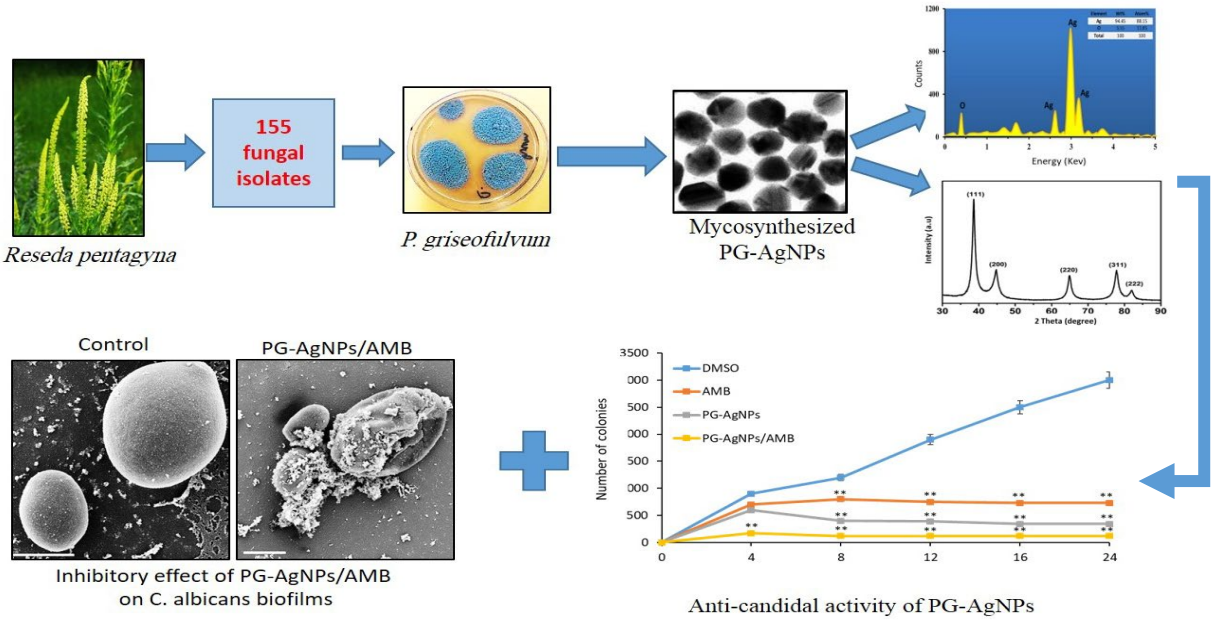

INTRODUCTION

Candida albicans may attack tissues by endocytosis or direct penetration under particular circumstances and stimulate injury of the epithelium tissue (Lu, 2021). *C. albicans* is one of the most public causes for invasive candidiasis with a mortality rate of 50% for systemic candidiasis patients (Şanlı et al., 2024). In immunocompromised people, it may result in obstinate infections of the oral cavity called oral candidiasis. About 80% of all women may be infected with vulvovaginal candidiasis, with 50%–60% feeling at least one extra incident of infection (Mayer et al., 2013). The pathogenicity of *C. albicans* is caused by virulence factors including biofilm formation, phospholipases secretion, adhesion, yeast-to-hyphal transition, and aspartyl proteases.

Resistance progress is the main problem for the therapeutic failure of antifungal drugs which are used against systemic candidiasis. This subject of antifungal resistance resulted in the development of multidrug-resistant fungal pathogens. Thus, the development of novel therapeutic antifungal agents is highly required to overcome the antifungal resistance (Lopes and Lionakis, 2022). The most different therapeutic choice in this current situation is the use of nanoscale materials as antifungal agents (Lee et al., 2021). The biosynthesis of nanoparticles NPs showed much consideration because of their distinctive physicochemical and biological characteristics. The green biosynthesis approaches include the use of plant extracts, microorganisms, or biomolecules as reducing and capping agents (Jain et al., 2021; Singh et al., 2023; Mohesien et al., 2023; Abd El Hamid et al., 2024; Amer, 2024). Recently, the effectual repression of *C. albicans* by green fabricated AgNPs was confirmed in this study as well using plant extracts of *Lotus lalambensis*, *Calotropis gigantean*, *Erodium glaucophyllum*, or *Artemisia annua* (Khatoon et al., 2019; Abdallah and Ali, 2021, 2022b). Despite hopeful records on using NPs as an antifungal drug against *C. albicans*, very scarce reports described the effect of mycosynthesized NPs as anti-candidal agents for the treatment of candidiasis.

Microorganisms such as bacteria, yeasts, algae, and fungi have always been capable of gathering and storing inorganic metallic ions from their environment. Therefore, the use of microorganisms may be the greatest alternate strategy of physical and chemical methods for the synthesis of NPs, as the green biosynthesis way is very spontaneous, cost effective, eco-friendly, and harmless (Chopra et al., 2022). Fungi may be defined as the best nanofactories compared to bacteria as they produce larger number of proteins, which directly lead to greater production of NPs (Kumari et al., 2023). In addition, they have high binding ability with metal ions in intracellular regions. Further, fungi can grow on the surface of inorganic substrate during culture and on solid substrate during fermentation resulting in the effectual dispersal of metals as a catalyst. Several reports defined the biological synthesis of AgNPs, but little is known about the prospective of fungi in this respect.

In this study, we aimed to use *Penicillium griseofulvum* for the mycosynthesis of AgNPs (PG-AgNPs). Our results revealed the synergism of the anti-candidal activity of PG-AgNPs in combination with Amphotericin B (PG-AgNPs/AMB) against candidiasis.

MATERIALS AND METHODS

Collection of Soil Samples

Reseda pentagyna rhizosphere soil samples (10 g) were gathered in clean sterilized dry polythene bags from a depth of 5 to 15 cm into the ground of those plants.

Isolation, Purification, and Identification of Fungi from the Rhizosphere

Different fungal species were isolated from the rhizospheres of *Reseda pentagyna* using serial dilution techniques (Waksman, 1922). Briefly, serial dilution of microbial suspensions was performed (10^{-1} to 10^{-6} µg/mL). Then, one mL of fungal suspension was transferred and placed in Petri plates containing sterilized PDA media (triplicate of each dilution) (Aziz and Zainol, 2018). The plates were incubated at 28°C for 7 days of incubation (Gaddeyya et al., 2012). Mixed fungal cultures were purified using the streak plate method (Maitig et al., 2018). Morphological identification of the isolated fungi was carried out at Al-Azhar University, Cairo, Egypt. All isolated fungi were screened for their anti-candidal activities in addition to the ability of their extracts to reduce $AgNO_3$ into AgNPs (data not shown). *Penicillium griseofulvum* F7 (RCMB 155) displayed a significant activity against *C. albicans* and a powerful potential to reduce $AgNO_3$ into AgNPs. Therefore, it was further selected for the mycosynthesis of PG-AgNPs.

Mycosynthesis of PG-AgNPs

The selected fungal isolate was cultivated on potato dextrose broth and incubated at 28°C under shaking at 100 rpm for 7 days. The fungal mycelia were filtered and washed with distilled water. 10 g of fungal mycelia was mixed with 100 mL of distilled water and incubated at 28°C for 72 h while shaking. Silver nitrate (1 mM) was mixed with 100 mL of fungal filtrate and incubated at 28°C for 24 h under dark conditions (Netala et al., 2016). The formation of AgNPs was verified by the conversion of color from colorless to reddish brown. The mycosynthesized AgNPs were stored at 4°C for further experiments.

Characterization of PG-AgNPs

UV-visible spectroscopy of PG-AgNPs was performed using the spectrophotometer Perkin Elmer (Abdallah and Ali, 2022a). PG-AgNPs coated on an XRD grid

were subjected to XRD examination in an X-ray diffractometer supplied with an operating voltage of 45 kV according to the method of Bahrami-Teimoori et al. (2017). The characterization of functional groups capped on PG-AgNPs was investigated by FTIR analysis (Shimadzu) at 4000 to 500 cm^{-1} using a Perkin Elmer infrared spectrophotometer (Abdallah and Ali, 2022a). EDX was performed using the energy dispersive X-ray technique (Model no. INCA 200, Oxford, UK). The zeta potential was measured by Zetasizer Nano Instrument (Malvern) (Abdallah and Ali, 2022a). The particle size of PG-AgNPs was evaluated by dynamic light scattering (DLS) measurements (Pradhan and Roy, 2013). TEM was achieved on JEOL (JEOL-JEM 1400, Freising, Germany) (Abdallah and Ali, 2022a).

Antifungal Activity of Silver Nanoparticles Biosynthesized by *Penicillium griseofulvum* (PG-AgNPs) against *C. albicans*

Anti-candidal activity of PG-AgNPs against *Candida albicans* (ATCC 14053, kindly provided by King Abdulaziz Hospital, National Guard Hospital in Al-Ahsa) was measured by the disc diffusion assay as described previously (Patra and Baek, 2017). The diameters of inhibition zones were determined after 48 h of incubation at 28°C.

Minimum Inhibitory Concentration (MIC): The MICs of PG-AgNPs and Amphotericin B were evaluated following the Clinical and Laboratory Standards Institute Document M38-A2 (Espinel-Ingroff et al., 2011). Briefly, serial bifold dilutions of PG-AgNPs and Amphotericin B were prepared at concentrations from 1 to 256 µg/mL. *C. albicans* was adjusted to 1×10^6 CFU and inoculated onto SDA plates containing different concentrations (256, 128, 64, 32, 16, 4, and 2 µg/mL) of PG-AgNPs and Amphotericin B (Abdallah and Ali, 2022a). The MIC refers to the lowest concentration of PG-AgNPs or Amphotericin B that did not display any growth of *C. albicans* on the plates (Kim et al., 2007).

Synergistic Antifungal Activity of PG-AgNPs/AMB against *C. albicans*: PG-AgNPs and Amphotericin B (1:1) (V/V) were mixed and sonicated for 15 min. Paper disks were saturated with 1 mL of the PG-AgNPs/AMB mixture solution. The synergistic effect was assessed by determining the diameter of inhibition zones (Ali and Abdallah, 2020).

Time-Kill Assay: The antifungal activities of PG-AgNPs, Amphotericin B, and PG-AgNPs/AMB were assessed at 0, 4, 8, 12, 16, and 24 h using the colony-counting assay. Counting the colonies formed was performed for an aliquot of 50 µL from each test suspension inoculated onto SDA (Mangoyi et al., 2015).

Effect of PG-AgNPs on the Virulence Factors of *C. albicans*

Dimorphic Transition: *C. albicans* was allowed to grow in RPMI-1640 with PG-AgNPs, Amphotericin B, and PG-AgNPs/AMB at 37°C for 24 h with consistent shaking at 120 rpm. A medium with dimethyl sulfoxide (DMSO) was considered as a negative control. After 24 h, *Candida* cells were collected and examined with a Digital Cell Imaging System in bright field as described (Manoharan et al., 2017).

Biofilm Establishment: *C. albicans* (1×10^5 cells/mL) was inoculated in RPMI-1640 and then added to 96-well microtiter plates. 50 µL of PG-AgNPs, Amphotericin B, and PG-AgNPs/AMB were added to wells that contained *C. albicans* cells and were incubated for 24 h. The plates were protected with parafilm and incubated for 24 h to allow biofilm establishment (Lara et al., 2015). The plates were washed with phosphate buffer saline to eliminate planktonic cells. Biofilm growth was evaluated by the MTT metabolic assay according to the method of Abdallah and Ali (2021).

Hydrolytic Enzymes: Activities of hydrolytic enzymes were evaluated according to the method of Santana et al. (2013). Briefly, *C. albicans* cells were exposed to PG-AgNPs. The proteinase enzyme activity was assessed by measuring the absorbance at 440 nm according to the method of Pande et al. (2006). The phospholipase enzyme activity was measured at 630 nm following the method of Gonçalves et al. (2012).

Antioxidant Enzymes: *C. albicans* were allowed to grow at 37°C with PG-AgNPs. The supernatant was scanned for antioxidant enzyme activities. Superoxide dismutase (SOD) was measured according to McCord and Fridovich (1969). Glutathione reductase (GSR) activity was measured as described by Carlberg and Mannervik (1985). Catalase (CAT) activity was determined following the method of Teranishi et al. (1974). Glucose-6-phosphate dehydrogenase (G6-P) activity was measured (Zaheer et al., 1967). The activity of glutathione peroxidase (GPX) was evaluated as described previously (Mohandas et al., 1984). Glutathione-S-transferase (GST) activity was measured as described by Habig et al. (1974).

Glucose and Trehalose Analysis*:* *C. albicans* were cultured in a PDA medium containing DMSO (negative control) and PG-AgNPs, Amphotericin B, and PG-AgNPs/AMB and incubated for 2 h at 28°C in PBS. *Candida* supernatants were mixed with 0.05 units of trehalase, and the enzymatic activity was performed for 1 h at 37°C. The mixture of glucose with the DNS reagent was boiled for 5 min and allowed to cool down, and then the color formed was measured at 525 nm as described (Kim et al., 2009).

Effect of PG-AgNPs on Ultrastructure Alterations of *C. albicans*

Scanning Electron Microscopy: *C. albicans* cells treated with PG-AgNPs, Amphotericin B, and PG-AgNPs/AMB were washed with phosphate-buffered saline (PBS) and fixed with 4% formaldehyde and 1% glutaraldehyde in PBS at RT. Samples were placed on copper grids for the evaluation of the ultrastructure by SEM using a Hitachi S-5500 as described (Lara et al., 2015).

Transmission Electron Microscopy: The TEM technique was used to examine the effects of PG-AgNPs, Amphotericin B, and PG-AgNPs/AMB on the ultrastructure of *C. albicans.* A suspension of *C. albicans* cells (10^5 CFU/mL) was mixed with PG-AgNPs and Amphotericin B, and PG-AgNPs/Amphotericin B was prepared. Ultrathin sections were obtained and observed by TEM using a JEM-ARM200F (JEOL USA Inc., MA, USA) as described (Vazquez-Muñoz et al., 2014).

Cell Culture and Cytotoxicity Assay: Primary mouse bone marrow-derived mesenchymal stem cells (mBMSCs) and human gingival fibroblast-1 (HGF-1) cell line were isolated as described previously (Abdallah et al., 2019). For cytotoxicity test, cells were treated with PG-AgNPs in 96-well plates at different concentrations for 48 h and cell viability was determined by the MTT cell proliferation test kit (Sigma-Aldrich), and optical density at 550 nm was measured using an ELISA plate reader as described (Abdallah and Ali, 2019).

Statistical Analysis

All values determined as mean ± SD (standard deviation), of 3 independent experiments. Power calculation was carried out for 2 samples by unpaired Student's *t*-test (2-tailed) using the Statistical Analysis Software package (SAS version 9.4; Cary, NC, USA), supposing equal difference in the two groups. *P<0.05 and **P<0.005 were considered significant.

RESULTS

Isolation and Purification of Fungi from Rhizosphere

In this study, soil around the rhizosphere of *Reseda pentagyna* was used to isolate fungi. We recovered 155 fungal isolates belonging to fifteen species represented by five diverse genera. *Aspergillus* and *Penicillium* were signified by more than three species among the isolates (Suppl. Table and Figure). The identified fungal species and their frequencies are recorded in Suppl. Table *Penicillium griseofulvum* was the leading isolated fungus with an occurrence frequency percentage of 13.2% of all isolates followed by *Aspergillus parasiticus* (12.2%), *Fusarium oxysporum* (12%), and *Aspergillus flavus* with the percentage of 10%. Conversely, the lowermost domination frequency that was documented is for *Penicillium citrinum* with 1.4% (Suppl. Table). The total colonization frequencies recorded were 52.7%, with 7% for *P. griseofulvum*, although the other fungal species documented colonization frequencies from 0.8% to 6%.

Mycosynthesis and Characterization of PG-AgNPs

PG-AgNPs were mycosynthesized from the fungal filtrate of *P. griseofulvum* (Figure 1A). The ability of the bioactive components of *P. griseofulvum* to act as biocatalysts for the reduction of Ag^+ to Ag^0 was evaluated. The color alteration of the biomass filtrate of *P. griseofulvum* after the addition of silver nitrate from colorless to reddish brown was identified (Figure 1A). This brown color represented the PG-AgNPs biosynthesis. The UV-visible spectra of biosynthesized PG-AgNPs showed a surface plasmon resonance absorption peak (SRP) at 426 nm (Figure 2A). The mycosynthesized PG-AgNPs were recognized in the form of nanocrystals by XRD. The XRD pattern revealed four diffraction peaks at 38.2°, 44.4°, 64.5°, 77.5°, and 81.6° at 2θ, corresponding to values of (111), (200), (220), (211), and (222) crystalline planes of cubic Ag (Figure 2B). The probable interaction among functional groups and PG-AgNPs was evaluated by FTIR examination. The data of FTIR designated the occurrence of carboxylic, hydroxyl, alkanes, and carbonyl groups on the surface of mycosynthesized PG-AgNPs. FTIR spectrum of PG-AgNPs showed peaks at 3432.94 cm^{-1} corresponding to the N–H stretching vibration of the primary and secondary amides of protein. The peak at 2777.28 cm^{-1} is attributed to single aldehyde. The peak at 2676.19 cm^{-1} is assigned to —C–H symmetrical stretching vibration of alkanes and O–H stretching of phenols and alcohols.

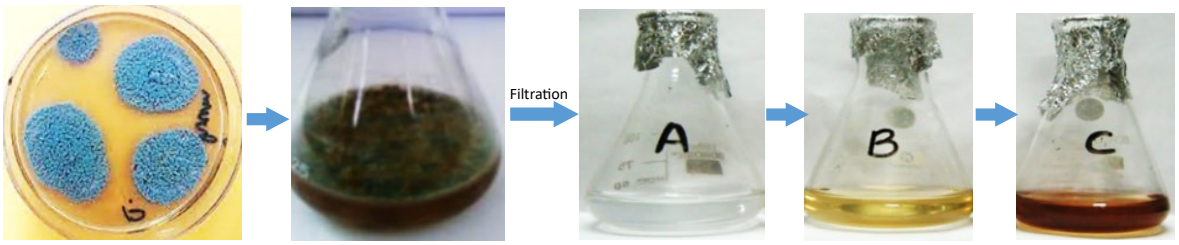

Figure 1. Biosynthesis of silver nanoparticles (PG-AgNPs) from cell-free filtrate (CFF) of *penicillium griseofulvum*. Color changes from light yellow to dark brown following the incubation at room temperature, indicating the reduction of the Ag^{+} ions and the biosynthesis of AgNPs.

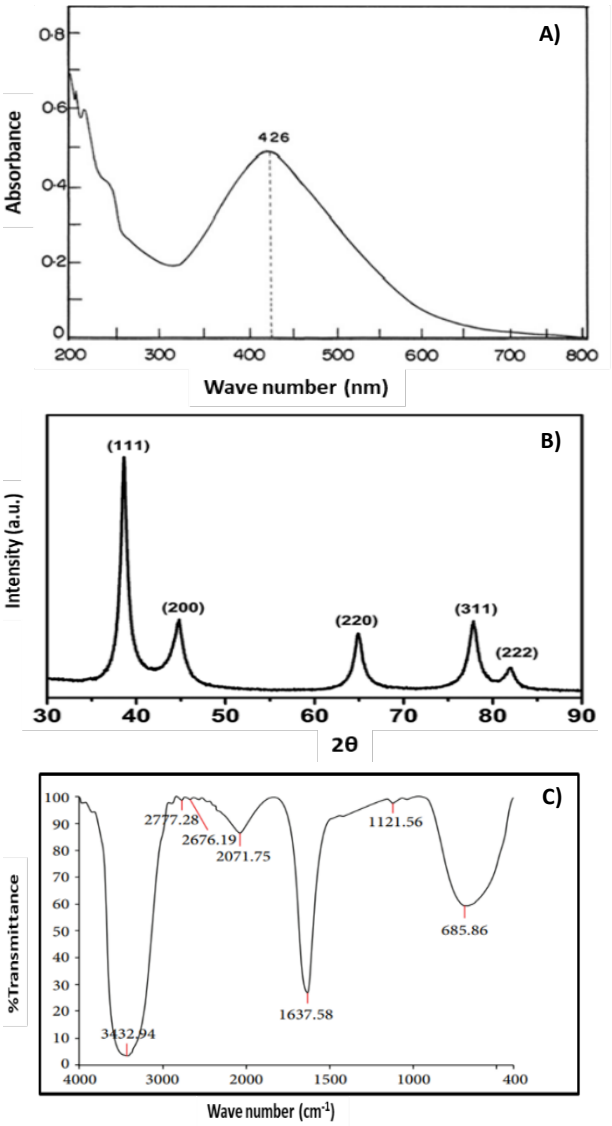

Figure 2. Confirmation of mycosynthesized silver nanoparticles (PG-AgNPs). (A) UV-Vis spectrum of PG-AgNPs. The highest absorbance peak was at about 426 nm, corresponding to the plasmon resonance of AgNPs. (B) XRD spectrum recorded for PG-AgNPs showed four distinct diffraction peaks at 38.2°, 44.4°, 64.5°, 77.5°, and 81.6° with indexed 2θ values of (111), (200), (220), (211), and (222) crystalline planes of cubic Ag. (C) FTIR spectrum of PG-AgNPs.

The peak at 2071.75 cm^{-1} corresponds to —C≡C stretching. The peak at 1637.58 cm^{-1} is related to —C=C stretching. The peak at 1121.56 cm^{-1} is associated with —C=O stretching (Figure 2C). DLS relies on the interaction of light with particles and is applied for the assessment of narrow particle size scatterings. After the analysis of PG-AgNPs by the DLS, it has been revealed that the size of colloidal PG-AgNPs is 50.4 nm (Figure 3A). The mycosynthesis of PG-AgNPs was further established by TEM, which showed the morphology of the PG-AgNPs to be spherical (Figure 3B). EDX revealed a weak peak for oxygen corresponding to the presence of Ag_2O (Figure 3C). The negative result of zeta potential verifies the repulsion between the particles, upsurges the constancy of the preparation in this manner, and prevents the nanoparticles from agglomeration, resulting in long-term constancy. The zeta potential of the PG-AgNPs was −10 mV (Figure 3D).

Antifungal Activity of PG-AgNPs against *C. albicans*

PG-AgNPs displayed a moderate anti-candidal activity at a concentration of 16 µg/mL with an inhibition zone of 27 mm as measured by the disk diffusion method. However, Amphotericin B at a concentration of 32 µg/mL showed lesser anti-candidal activity with an inhibition zone of 23 mm (Figure 4A&B).

Synergistic Antifungal Activity of PG-AgNPs/AMB on *C. albicans*

As shown in Figure 4A, PG-AgNPs/AMB showed significant synergistic anti-candidal activity against *C. albicans*, with a zone of inhibition of 35 mm. Moreover, the fungistatic activity of Amphotericin B and PG-AgNPs was detected at 32 and 16 µg/mL, respectively, as assessed by the time-kill tests (Figure 4C). The growth of *C. albicans* cells was inhibited by PG-AgNPs/AMB after 4 h of incubation (Figure 4C).

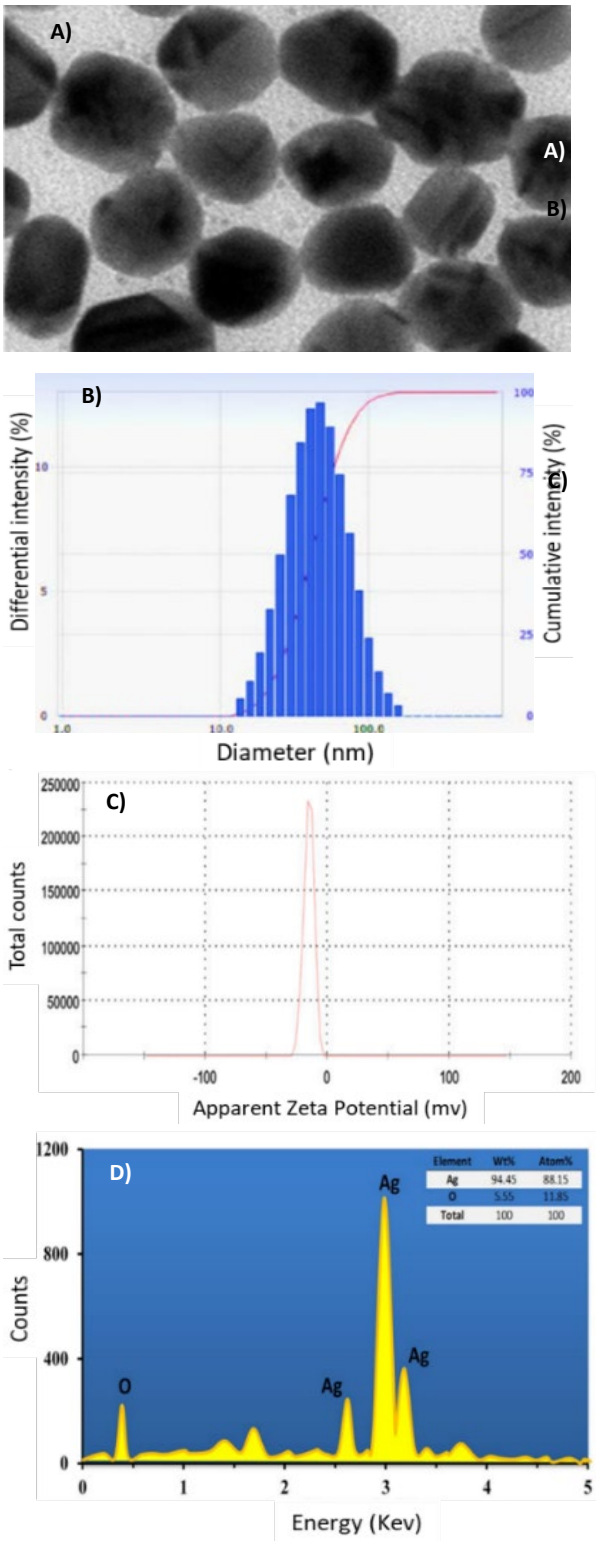

Figure 3. Transmission electron microscopy (TEM) image (A) and dynamic light scattering (DLS) histogram analyses (B) of PG-AgNPs. Zeta potential of mycosynthesized silver nanoparticles (C) and EDX spectrum of PG-AgNPs (D). According to TEM, PG-AgNPs are in spherical shape with 10-40 nm diameter. The average size of colloidal PG-AgNPs is 50.4 nm as shown by the DLS analysis.

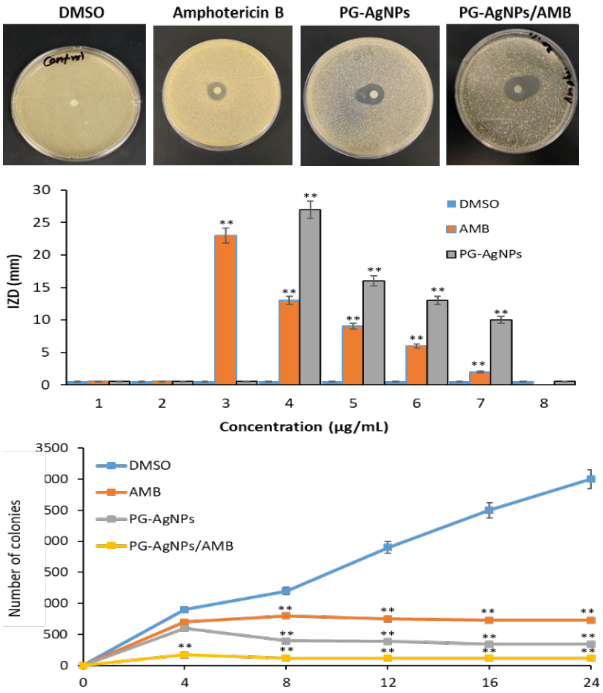

Figure 4. Antimicrobial potential of PG-AgNPs. (A) Disc diffusion method showing the anti-candidal activity of PG-AgNPs and the synergistic anti-candidal potential of PG-AgNPs (16 µg/mL) mixed with Amphotericin B (32 µg/mL). (B) Anti-candidal activity of PG-AgNPs and Amphotericin B on *C. albicans*. IZD = inhibition zone diameter (mm). Data are expressed as the mean zone of inhibition in mm. (C) Time-kill curves of *C. albicans* following the exposure to PG-AgNPs, Amphotericin B, and PG-AgNPs/AMB. Values are means ± SD (**P < 0.005, compared to control DMSO-treated cells).

Thus, PG-AgNPs/AMB showed a superior anti-candidal potential to PG-AgNPs or Amphotericin B alone.

PG-AgNPs/AMB Inhibits the Virulence Factors of *C. albicans*

As displayed in Figure 5A and Table 1, the non-treated controls (DMSO) of *C. albicans* cells showed great growth of hyphae after 24 h. On the other hand,
hyphal growth was totally inhibited after the exposure to PG-AgNPs/AMB (16/32 µg/mL) as examined using phase contrast microscopic observations. Furthermore, we observed the anti-adhesive and anti-biofilm efficacy of PG-AgNPs, Amphotericin B, and PG-AgNPs/AMB. PG-AgNPs (16 µg/mL) repressed the adherence and biofilm establishment of *C. albicans* by 60% and 55%, respectively, whereas PG-AgNPs/AMB (16/32 µg/mL) repressed the adherence and biofilm establishment of *C. albicans* by 92% and 88%, respectively (Figure 5B&C).

PG-AgNPs Suppresses the Hydrolytic Enzymatic Activities

C. albicans-produced hydrolytic enzymes were assessed by the proteinase and phospholipase enzyme assays. PG-AgNPs/AMB (16/32 µg/mL) expressively decreased the enzyme activities of proteinases and phospholipases by 75% and 78%, respectively (Figure 5D&E).

PG-AgNPs Raises the Intracellular Glucose and Trehalose Discharge

C. albicans cells exposed to Amphotericin B or PG-AgNPs accumulated extra intracellular glucose and trehalose than control. Moreover, these cells also have higher trehalose and extracellular glucose as compared to DMSO-treated cells (Figure 5F&G). Remarkably, the maximum production of extracellular glucose and trehalose (2 µg per fungal dry weight of 1 mg) was detected for PG-AgNPs/AMB. This rate was expressively greater than PG-AgNPs or Amphotericin B treatments (28.9 and 31.5 µg/mg, respectively).

PG-AgNPs Suppressed the Secretion of Antioxidant Enzymes by *C. albicans*

We studied the inhibitory effect of PG-AgNPs/AMB on the activity of antioxidant enzymes by *C. albicans*. Table 3 shows the significant suppression effect of PG-AgNPs/AMB on the following antioxidant-related enzymes, including GST, CAT, SOD, G6-P, GSR, and GPX by 84.72%, 85.91%, 86.23%, 85.51%, 84.73%, and 100%, respectively (Table 2).

Ultrastructural Imaging of *C. albicans* Treated with PG-AgNPs Using SEM and TEM Investigation

PG-AgNPs/AMB treatment revealed obvious morphological alterations. Treated cells displayed a rugged surface and detachment of the outer layer of the yeast cell wall. Additionally, masses of cellular debris were observed (Figure 6A, c–f). Control non-treated cells exhibited a normal morphology with multiple organelles of *Candida* cells as assessed by TEM (Figure 6B, a–d). In contrast, cells exposed to PG-AgNPs/AMB exhibited disconcertion of the cell wall, disturbance of the cell membrane, and development of holes with a whole damage of the cells. In addition, we detected a contraction of the cytoplasm from the cell wall and a leakage of the intracellular substances from the cells, which resulted in cell death (Figure 6B, e–m).

Effect of PG-AgNPs/AMB on Biofilm Ultrastructure using SEM

Scanning electron microscopy (SEM) images were performed for biofilms, allowed to grow for 48 h in RPMI 1640, and then treated with PG-AgNPs/AMB for another 24 h. Main imperfections were detected in biofilm structure after the treatment with PG-AgNPs/AMB. The results showed deep wrinkles and deformity in hyphal structures, hyphal networks had collapsed, and hyphal tips presented marks of impairment (Figure 6C a,b), while control cells retained a normal form and hyphae appeared intact and unaffected (Figure 6C c, d).

PG-AgNPs Display No Cytotoxicity on Animal and Human Cells

PG-AgNPs did not show any signs of cytotoxicity on both mBMSCs and human HGF-1 cells up to 120 and 150 µg/mL, respectively. As shown in Figure 7A&B, PG-AgNPs started to affect the cell viability at 150 and 200 µg/mL on mBMSCs and human HGF-1, respectively (Figure 7A&B).

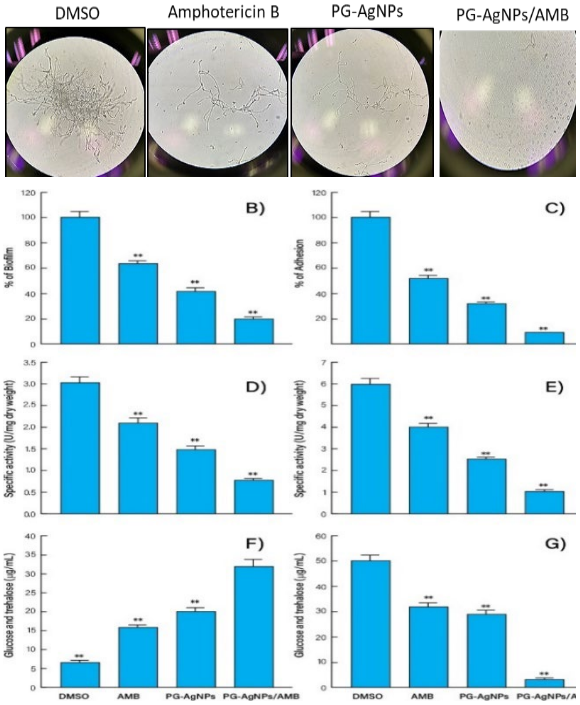

Figure 5. Effect of PG-AgNPs on dimorphic transition of *C. albicans* (A). Effect of PG-AgNPs on adhesion (after two hours, C) and biofilm formation (after 24 hours) of *C. albicans*. (D) Proteinase enzyme activity after treatment with PG-AgNPs (16 µg/mL)/AMB (32 µg/mL) displayed 75% inhibition of enzyme activity. (E) Phospholipase enzyme activity after treatment with PG-AgNPs (16 µg/mL)/AMB (32 µg/mL) showed up to 78% reduction of enzyme activity. (F) The concentration of intracellular trehalose and glucose of *C. albicans*. (G) The concentrations of extracellular trehalose and glucose from *C. albicans*. Values are means ± SD (**P < 0.005, compared to control DMSO-treated cells.

Table 1. Anti-candidal activity of PG-AgNPs and amphotericie b *C. albicans.*

Concentration (µg/ml)	Antifungal agent		
	DMSO	AMB	PG-AgNPs
	IZD (mm)		
0	a0^{a}±0.0	a0^{a}±0.0	a0^{a}±0.0
2	a0^{a}±0.0	b2^{b}±0.7	b10^{c}±0.7
4	a0^{a}±0.0	c6^{b}±0.5	c13^{c}±0.5
8	a0^{a}±0.0	d9^{b}±0.5	d16^{c}±0.8
16	a0^{a}±0.0	e13^{b}±0.5	e27^{c}±0.8
32	a0^{a}±0.0	f23^{b}±0.5	**No growth**
64	a0^{a}±0.0	**No growth**	
128	a0^{a}±0.0		

IZD= IZD-IZD=Inhibition zone diameter (mm). Data are expressed as the mean zone of inhibition in mm followed by SD. The values with different subscript letters in the same column and those with different superscript letters in the same raw are significantly different according to ANOVA and Duncan's multiple range tests.

Table 2. Effect of PG-AgNPs, Amphotericin B, and PG-AgNPs/AMB on dimorphic transition of *C. albicans.*

Antifungal agent	YF count (cell/ mL)	FF count (cell /mL)	% of dimorphism
DMSO	86^{b}±3.0	1850^{d} ±2.0	95.35±2.5
Amphotericin b	556^{d}±4.0	1100^{c}±6.0	49.45±0.9
PG-AgNPs	299^{c}±2.0	514^{b} ±0.5	41.82±0.6
PG- AgNPs/AMB	22^{a}±1.5	28^{a}±0.83	21.42±0.5

Data are expressed as the mean zone of inhibition in mm followed by SD. The values with different superscript letters in the same column are significantly different according to ANOVA and Duncan's multiple range tests. % of dimorphism is calculated as per the following equation: % of dimorphism = FF-YF/FF × 100, wherein YF is the yeast form and FF is the filamentous form.

Table 3. Specific activities of antioxidant enzymes.

Enzyme	Substrate	Specific activity (U/mg protein)	
		Control	PG-AgNPs/AMB
Glutathione-S Transferase	CDNB	0.833 ± 0.21	0.0954 ± 0.001
Catalase	H_2O_2	4.5 ± 0.23	0.72 ± 0.15
Superoxide dismutase	Epinephrine	0.903 ± 0.05	0.0221 ± 0.014
Glucose-6-phosphate dehydrogenase	NADP	645.24 ± 6.11	64.134 ± 1.5
Glutathione reductase	NADPH	77.21 ± 3.123	8.13 ± 0.33
Glutathione peroxidase	NADPH	0.00066 ± 0.0001	0.00022 ± 0.0

DISCUSSION

The rhizosphere is the soil region around the roots of plants that is directly affected by soil fungi and plant root exudates. Rhizospheric fungi are also recognized as an important source of several bioactive metabolites that support plant growth (Müller et al., 2016). In this study, 155 fungal isolates were recovered from the rhizosphere of *Reseda pentagyna*. The fungus *Penicillium griseofulvum* was the predominant isolated fungus. Several studies described the isolation of different fungi from the rhizosphere soil. For example, Talukdar et al. (2021) isolated *Colletotrichum* sp. from the rhizosphere of *Houttuynia cordata*. Similarly, Kumari et al. (2021) isolated *Penicillium citrinum* from the rhizosphere of *Azadirachta indica.* Additionally, 15 fungal species were previously isolated from the rhizosphere of *Ephedra pachyclada* identified as *Penicillium crustosum*, *Penicillium commune*, *Penicillium corylophilum*, *Penicillium caseifulvum*, *Alternaria tenuissima* (EP-13), *Aspergillus flavus*, and *Aspergillus niger* (Khalil et al., 2021).

In this research, we are the first to apply *P. griseofulvum* in the mycosynthesis of AgNPs. The UV-visible spectra of mycosynthesized PG-AgNPs showed an absorption band at 426 nm. PG-AgNPs were displayed in the form of nanocrystals by XRD with an average size of 50.4 nm. Our data are in agreement with Iqtedar et al. (2019) who mycosynthesized AgNPs from *Aspergillus sydowii* which showed a strong absorbance peak at 420 nm with crystalline features.

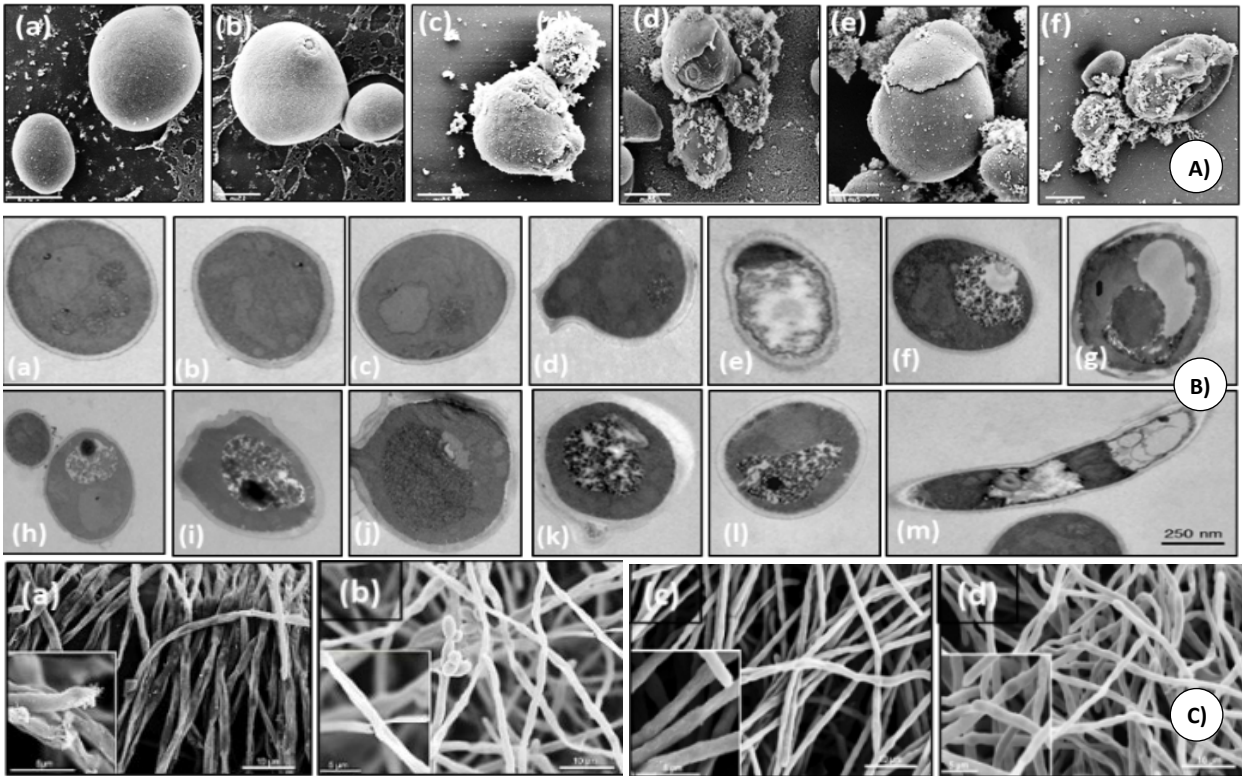

Figure 6. Ultrastructure modifications of *C. albicans* after exposure to PG-AgNPs/AMB. (A) Scanning electron microscopy of *C. albicans* cells treated with PG-AgNPs/AMB. Approximately, 10^8 yeast cells were incubated without (a, b) or with (c-f) PG-AgNPs (16 µg/mL)/AMB (32 µg/mL) for 2h. (B) Transmission electron microscopy photographs of *C. albicans* cells treated with PG-AgNPs/AMB. Approximately 10^8 yeast cells were incubated without (a–d) or with (e–m) PG-AgNPs (16 µg/mL)/AMB (32 µg/mL) for 2h. (C) SEM images of *C. albicans* biofilms which were grown for 42 h in RPMI at pH 7.4 and then exposed to PG-AgNPs/AMB for another 24 h (a, b). Control images were taken of biofilms grown in RPMI medium without PG-AgNPs/AMB (c, d). Insets show hyphal structures in detail. Scale bars indicate 10 mm in main images and 5 mm in insets.

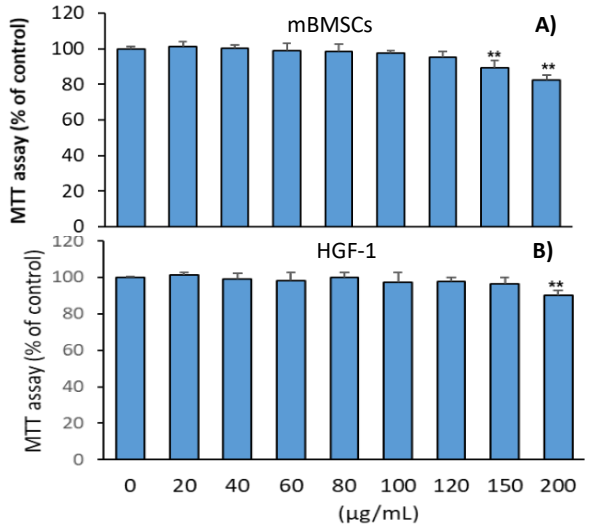

Figure 7. Effect of PG-AgNPs on animal cells. Cytotoxicity of PG-AgNPs on primary mBMSCs (A) and human HGF-1 cell line (B). The dose-dependent effect of PG-AgNPs on cell viability measured by MTT assay after 48 h of treatment. Values are expressed as mean ± SD of three independent experiments. (**P < 0.005, compared to control non-treated cells).

Similarly, Othman et al. (2016) mycosynthesized spherical-shape AgNPs from *Aspergillus fumigatus* with a distinct and typical SPR band in the region of 410 nm of diameter range between 10 and 34 nm. They also biosynthesized AgNPs from *Penicillium politans* NRC510 filtrates with a characteristic and well-defined SPR band obtained at around 433 nm (Othman et al., 2016).

Although the precise mechanistic action of mycosynthesis of NPs is not clear, it was reported that the supernatant of fungi might act as reducing and capping mediators due to the presence of biomolecules such as proteins, amino acids, enzymes, vitamins, and polysaccharides (Gudikandula et al., 2017). More specifically, enzyme nicotinamide adenine dinucleotide (NADH) and NADH-dependent nitrate reductase seemed to mediate the synthesis of AgNPs from $AgNO_3$ (Anil Kumar et al., 2007; Kalimuthu et al., 2008).

The results of the disk diffusion method revealed moderate antifungal activity of PG-AgNPs at 16

µg/mL. Several authors previously described the antifungal activity of green biosynthesized AgNPs (Lin et al., 2021; Mabrouk et al., 2021; Zwar et al., 2023). Our results went in parallel with Ribeiro et al. (2023) who revealed that AgNPs mycosynthesized using *Aspergillus* spp. presented an anti-candidal activity against several clinical strains of *Candida* including *C. albicans*, with MICs in the range from 1.25 to 40 µM. Similarly, AgNPs mycosynthesized by *Aspergillus sydowii* cell filtrate showed an anti-candidal activity against *Candida* spp. with an MIC range from 100 to 200 µg/mL (Wang et al., 2021). In this context, Ali and Abdallah (2020) displayed that AgNPs biosynthesized from *C. gigantea* displayed a higher antifungal potential against *C. albicans* with an MIC of 100 µg/mL. Furthermore, the EG-AgNPs biosynthesized using *Erodium glaucophyllum* exhibited a higher anti-candidal activity compared to Amphotericin B wherein the MIC values of EG-AgNPs and Amphotericin B were 50 and 100 µg/mL, respectively (Abdallah and Ali, 2022a).

AgNPs are reported to exert an anti-candidal effect by increasing the membrane permeability barrier and lipid bilayers, leading to the leakage of ions and disintegrating the electrical potential of the membrane. In addition, AgNPs showed the ability to block the cell cycle in *C. albicans* at the G2/M phase (Kim et al., 2009), resulting in increased reactive oxygen species (ROS) and reduced antioxidant enzymes (Dantas Ada et al., 2015).

Interestingly, PG-AgNPs/AMB displayed a higher synergistic antifungal activity against *C. albicans*. Our results went in parallel with Jia and Sun (2021) who indicated that AgNPs worked synergistically with fluconazole against fluconazole-resistant *C. albicans*. Similarly, Murray et al. (1995) determined the synergistic antifungal activity of AgNPs and Amphotericin B against *Candida* species. They found that the AgNPs (50 µg/mL) did not display any anti-candidal activity against *the Candida* species. However, when AgNPs were mixed with a standard anti-candidal drug, Amphotericin B, they showed a powerful anti-candidal activity against *Candida* species, with inhibition zones of 9.74 to 14.75 mm (Murray, 1995).

Few studies described the mode of action of the combination of NPs and antifungal drugs. For example, AgNPs/miconazole displayed an antifungal effect via the accumulation of ROS and the inhibition of ergosterol synthesis (Kumar and Poornachandra, 2015). Furthermore, the antifungal effect of AgNPs/fluconazole was reported to be due to the inhibition of ergosterol pathway and efflux pumps (Sun et al., 2016).

Dimorphic transition is considered as the most important factor in stimulating epithelial invasion, which activates the deprivation of epithelial cell junction proteins (Villar et al., 2007; Mech et al., 2014). Our results confirmed the blocking of hyphal growth by PG-AgNPs/AMB. Our data are consistent with those of Jalal et al. (2019) who found that Sc-AgNPs biosynthesized using seed extract of *Syzygium cumini* completely inhibit the morphogenesis of *C. albicans* in a dose-dependent manner.

The mode of action of NPs to inhibit the dimorphic transition of *C. albicans* is not clear. AgNPs showed an ability to disturb the Ras-mediated signal transduction pathways in *C. albicans* by downregulating the expression of hyphal inducer gene (TEC), yeast-to-hyphal transition genes (TUP1 and RFG1), and cell elongation gene (ECE1) (Różalska et al., 2014). In addition, AgNPs may direct regulatory networks such as environmental sensing, signaling, and transcriptional modulators in addition to chromatin alterations which play a significant role in the dimorphic transition and pathogenicity (Maubon et al., 2014; Rajendran et al., 2016).

C. albicans has the capability to form biofilms that support their adherence to surfaces and surge their resistance to antifungal drugs (Forsberg et al., 2019). Our results revealed that PG-AgNPs/AMB repressed the adhesion and biofilm formation by 92% and 88%, respectively. Lara et al. (2015) reported a dose-dependent suppression effect of AgNPs on biofilm formation, with an IC_{50} of 0.089 ppm. Similarly, AgNPs at 1/2 MIC, MIC, and 2MIC displayed an inhibition in the formation of the biofilm of *C. albicans* by 10%, 35%, and 62.5%, respectively (Ahamad et al., 2021). The precise mode of action that AgNPs constrain biofilm formation is unidentified. Różalska et al. (2018) suggested that the anti-biofilm effect of AgNPs may be owing to the binding of AgNPs and dissemination into the biofilm, disturbing the lipidome of cell membranes. Another probable mechanism comprises the inhibition of hyphal development by AgNPs and the breakdown of the cell wall, which permits yeast and filamentous *Candida* spp. to live (Lara et al., 2015; Różalska et al., 2018).

Our results of SEM and TEM for PG-AgNPs-treated cells are consistent with those of Lara et al. (2015) where their TEM images revealed that *C. albicans*

cells treated with AgNPs for 24 h at 0.089 ppm were mostly distended, with modifications in both cell membrane and cell wall. In this context, major changes in the structure of *C. albicans* cells were reported for biosynthesized AgNPs (Radhakrishnan et al., 2018; Jalal et al., 2019; Abdallah and Ali, 2022a).

PG-AgNPs/AMB showed an inhibitory effect on the activities of antioxidant enzymes. AgNPs were reported to display an antioxidant potential via the stimulation of *C. albicans* to express genes encoding components of the thioredoxin systems and antioxidant enzymes (Rahimi-Nasrabadi et al., 2014; Dantas Ada et al., 2015). Our results are in agreement with Ali and Abdallah (2020) who found that AgNPs presented the capability to expressively constrain the following antioxidant-related enzymes in *C. albicans*. Similarly, Fang et al. (2019) investigated the effects of AgNPs on the activities of antioxidant enzymes in vitro and reported a dose-dependent inhibitory effect on CAT enzymes.

The disturbance of the cell membrane by AgNPs resulted in the discharge of glucose and trehalose. Trehalose interacts with phospholipids on the cell membrane and defends fungi against several stress circumstances (Miao et al., 2016). Our results demonstrated high induction of extracellular glucose and trehalose from *C. albicans* cells by PG-AgNPs/AMB and in agreement with previous studies demonstrating the stimulatory effect of green AgNPs on accumulating the intracellular glucose and trehalose on *C. albicans* (Abdallah and Ali, 2021).

Our results revealed that PG-AgNPs/AMB significantly inhibit the enzyme production of proteinases and phospholipases. Phospholipases are related to adhesion, initiation of germ tubes, morphogenesis, penetration, and tissue damage. Similar results were formerly described by Hamid et al. (2018) who reported that AgNPs mycosynthesized by *Aspergillus* spp. constrain the production of phospholipases in *Candida*. In this context, Jalal et al. (2018) found that ZnONPs biosynthesized by an extract of *Crinum latifolium* decreases the production of phospholipases in *C. albicans*. Our results are also consistent with those of Jalal et al. (2019) who established the inhibitory activities of green biosynthesized Sc-AgNPs on the secretion of phospholipases by five *Candida* spp.

Interestingly, PG-AgNPs did not show any signs of cytotoxicity on either mBMSCs or human HGF-1 cells. This data is in consistence with green synthesized AgNPs using wild plants extracts (Alsalhi et al., 2016; Lee and Jun, 2019; Ali and Abdallah, 2020, 2021).

CONCLUSION

In this research, we mycosynthesized AgNPs using the cell-free filtrate of *P. griseofulvum*. Our data confirmed the efficient antifungal prospective of a combination of mycosynthesized AgNPs and Amphotericin B (PG-AgNPs/AMB). PG-AgNPs/AMB significantly inhibited growth, morphogenesis, biofilm development, and activity of antioxidant enzymes of *C. albicans* without showing any cytotoxicity at MIC concentrations. Thus, we identified PG-AgNPs/AMB as a plausible novel therapeutic approach for candidiasis.

ACKNOWLEDGMENTS

This work was supported by the Deanship of Scientific Research, Vice Presidency for Graduate Studies and Scientific Research, King Faisal University, Saudi Arabia (Grant no. KFU242129).

CONFLICT OF INTERESTS

The authors declare that they have no competing interests.

REFERENCES

Abdallah, B.M., Ali E.M. (2019) 5'-hydroxy Auraptene stimulates osteoblast differentiation of bone marrow-derived mesenchymal stem cells via a BMP-dependent mechanism. *Journal of biomedical science*, 26,51-63

Abdallah, B.M., Ali, E.M. (2021) Green Synthesis of Silver Nanoparticles Using the Lotus lalambensis Aqueous Leaf Extract and Their Anti-Candidal Activity against Oral Candidiasis. *ACS omega*, 6,8151-8162

Abdallah, B.M., Ali, E.M. (2022a) Therapeutic Effect of Green Synthesized Silver Nanoparticles Using Erodium glaucophyllum Extract against Oral Candidiasis: In Vitro and In Vivo Study. *Molecules*, 27,4221-4235

Abdallah, B.M., Ali, E.M. (2022b) Therapeutic Potential of Green Synthesized Gold Nanoparticles Using Extract of Leptadenia hastata against Invasive Pulmonary Aspergillosis. *Journal of fungi (Basel, Switzerland),* 8(5),442-435

Abdallah, B.M., Alzahrani, A.M., Abdel-Moneim, A.M., Ditzel, N., Kassem, M. (2019) A simple and reliable protocol for long-term culture of murine bone marrow stromal (mesenchymal) stem cells that retained their in vitro and in vivo stemness in long-term culture. *Biological procedures online,* 21,3-14

Abd El Hamid, D., Desouky, E., AbdEllatif, S., Abed, N., Mahfouz, A. (2024). Green Synthesis and Characterization of Titanium Dioxide Nanoparticles by

Aspergillus niger DS22 and Its Potential Application in Medical Fields. Egyptian Journal of Botany, 64(2), 629-653. doi: 10.21608/ejbo.2024.245157.2550

Ahamad, I., Bano F., Anwer, R., Srivastava, P., Kumar R., Fatma, T. (2021) Antibiofilm Activities of Biogenic Silver Nanoparticles Against Candida albicans. *Front Microbiol* 12,741493-741503

Amer, H. (2024). Green Synthesized ZnO Nanoparticles Improve the Growth and Phytohormones Biosynthesis and Modulate the Expression of Resistance Genes in Phaseolus vulgaris. Egyptian Journal of Botany, 64(1), 145-163. doi: 10.21608/ejbo.2023.218237.2383.

Ali, E.M., Abdallah, B.M. (2020) Effective Inhibition of Candidiasis Using an Eco-Friendly Leaf Extract of Calotropis-gigantean-Mediated Silver Nanoparticles. *Nanomaterials (Basel, Switzerland)* 10,422-435

Ali, E.M., Abdallah, B.M. (2021) Effective Inhibition of Invasive Pulmonary Aspergillosis by Silver Nanoparticles Biosynthesized with Artemisia sieberi Leaf Extract. *Nanomaterials (Basel, Switzerland)* 12,51-63

Alsalhi, M.S., Devanesan, S., Alfuraydi A.A., et al. (2016) Green synthesis of silver nanoparticles using Pimpinella anisum seeds: antimicrobial activity and cytotoxicity on human neonatal skin stromal cells and colon cancer cells. *International journal of nanomedicine* 11,4439-4449

Anil Kumar, S., Abyaneh, M.K., Gosavi, S.W., et al. (2007) Nitrate reductase-mediated synthesis of silver nanoparticles from AgNO3. *Biotechnol Lett*, 29(3):439-445

Aziz N.H., Zainol N. (2018) Isolation and identification of soil fungi isolates from forest soil for flooded soil recovery. *IOP Conference Series: Materials Science and Engineering* 342

Bahrami-Teimoori, B., Nikparast, Y., Hojatianfar, M., Akhlaghi, M., Ghorbani R., Pourianfar H.R. (2017) Characterisation and antifungal activity of silver nanoparticles biologically synthesised by Amaranthus retroflexus leaf extract. *Journal of Experimental Nanoscience,* 12,129 - 139

Carlberg, I., Mannervik, B. (1985) Glutathione reductase. *Methods in enzymology* 113,484-90

Chopra, H., Bibi, S., Singh, I., et al. (2022) Green Metallic Nanoparticles: Biosynthesis to Applications. *Front Bioeng Biotechnol,* 10:874742

Dantas Ada, S., Day A., Ikeh, M., Kos I., Achan, B., Quinn, J. (2015) Oxidative stress responses in the human fungal pathogen, Candida albicans. *Biomolecules* 5(1):142-165

Espinel-Ingroff, A., Cuenca-Estrella, M., Fothergill A., et al. (2011) Wild-type MIC distributions and epidemiological cutoff values for amphotericin B and Aspergillus spp. for the CLSI broth microdilution method (M38-A2 document). *Antimicrobial agents and chemotherapy*, 55(11):5150-5154

Fang W., Chi Z, Li W., Zhang X., Zhang Q. (2019) Comparative study on the toxic mechanisms of medical nanosilver and silver ions on the antioxidant system of erythrocytes: from the aspects of antioxidant enzyme activities and molecular interaction mechanisms. *Journal of Nanobiotechnology,* 17(1):6674

Forsberg, K., Woodworth, K., Walters, M., et al. (2019) Candida auris: The recent emergence of a multidrug-resistant fungal pathogen. *Med Mycol,* 57(1):1-12

Gaddeyya G., Niharika P.S., Bharathi P., Kumar P.K.R. (2012) Isolation and identification of soil mycoflora in different crop fieldsat Salur Mandal. *Advances in Applied Science Research* 3

Gonçalves L.M., Del Bel Cury A.A., Sartoratto A., Garcia Rehder V.L., Silva W.J. (2012) Effects of undecylenic acid released from denture liner on Candida biofilms. J*ournal of dental research*, 91(10),985-9

Gudikandula K., Vadapally P., Charya M.A.S. (2017) Biogenic synthesis of silver nanoparticles from white rot fungi: Their characterization and antibacterial studies. *OpenNano*, 2:64-78

Habig W.H., Pabst M.J., Jakoby W.B. (1974) Glutathione S-transferases. The first enzymatic step in mercapturic acid formation. *The Journal of biological chemistry,* 249(22),7130-9

Hamid S., Zainab S., Faryal R., Ali N., Sharafat I. (2018) Inhibition of secreted aspartyl proteinase activity in biofilms of Candida species by mycogenic silver nanoparticles. *Artificial cells, nanomedicine, and biotechnology,* 46(3),551-557

Iqtedar M., Aslam M., Akhyar M., Shehzaad A., Abdullah R., Kaleem A. (2019) Extracellular biosynthesis, characterization, optimization of silver nanoparticles (AgNPs) using Bacillus mojavensis BTCB15 and its antimicrobial activity against multidrug resistant pathogens. *Prep Biochem Biotechnol,* 49(2),136-142

Jain A.S., Pawar P.S., Sarkar A., Junnuthula V., Dyawanapelly S. (2021) Bionanofactories for Green Synthesis of Silver Nanoparticles: Toward Antimicrobial Applications. *International journal of molecular sciences,* 22(21),11993-12005

Jalal M., Ansari M.A., Ali S.G., Khan H.M., Rehman S. (2018) Anticandidal activity of bioinspired ZnO NPs: effect on growth, cell morphology and key virulence attributes of Candida species. *Artif Cells Nanomed Biotechnol,* 46(sup1),912-925

Jalal M., Ansari M.A., Alzohairy M.A., et al. (2019) Anticandidal activity of biosynthesized silver nanoparticles: effect on growth, cell morphology, and key virulence attributes of Candida species. *International journal of nanomedicine,* 14,4667-4679

Jia D., Sun W. (2021) Silver nanoparticles offer a synergistic effect with fluconazole against fluconazole-resistant Candida albicans by abrogating drug efflux pumps and increasing endogenous ROS. Infection, genetics and evolution : *journal of molecular epidemiology and*

evolutionary genetics in infectious diseases, 93,104937

Kalimuthu K, Suresh Babu R, Venkataraman D, Bilal M, Gurunathan S (2008) Biosynthesis of silver nanocrystals by Bacillus licheniformis. Colloids and surfaces B, Biointerfaces 65(1):150-3 doi:10.1016/j.colsurfb.2008.02.018

Khalil A.M.A., Hassan S.E., Alsharif S.M., et al. (2021) Isolation and Characterization of Fungal Endophytes Isolated from Medicinal Plant Ephedra pachyclada as Plant Growth-Promoting. *Biomolecules*, 11(2), 140-153

Khatoon N., Sharma Y., Sardar M., Manzoor N. (2019) Mode of action and anti-Candida activity of Artemisia annua mediated-synthesized silver nanoparticles. *Journal de mycologie medicale*, 29(3),201-209

Kim J.H., Campbell B.C., Mahoney N., Chan K.L., Molyneux R.J., May G.S.. (2007) Enhanced activity of strobilurin and fludioxonil by using berberine and phenolic compounds to target fungal antioxidative stress response. *Letters in applied microbiology,* 45(2),134-41

Kim K.J., Sung W.S., Suh B.K., et al. (2009) Antifungal activity and mode of action of silver nano-particles on Candida albicans. *Biometals : an international journal on the role of metal ions in biology, biochemistry, and medicine,* 22(2),235-42

Kumar C.G., Poornachandra Y. (2015) Biodirected synthesis of Miconazole-conjugated bacterial silver nanoparticles and their application as antifungal agents and drug delivery vehicles. *Colloids Surf B Biointerfaces,* 125,110-9

Kumari S., Raturi S., Kulshrestha S., et al. (2023) A comprehensive review on various techniques used for synthesizing nanoparticles. *Journal of Materials Research and Technology*, 27,1739-1763

Lara H.H., Romero-Urbina D., Pierce C.G., Lopez-Ribot J.L., Arellano-Jimenez M.J., José-Yacamán M. (2015) Effect of silver nanoparticles on Candida albicans biofilms: an ultrastructural study. *Journal of Nanobiotechnology,* 13, 91-102

Lee S.H., Jun B.H. (2019) Silver Nanoparticles: Synthesis and Application for Nanomedicine. *International journal of molecular sciences*, 20(4),865-882

Lee Y., Puumala E., Robbins N., Cowen L.E. (2021) Antifungal Drug Resistance: Molecular Mechanisms in Candida albicans and Beyond. *Chem Rev,* 121(6),3390-3411

Lin Y., Betts H., Keller S., Cariou K., Gasser G. (2021) Recent developments of metal-based compounds against fungal pathogens. Chem Soc Rev 50(18):10346-10402

Lopes JP, Lionakis MS (2022) Pathogenesis and virulence of Candida albicans. *Virulence,* 13(1),89-121

Lu S-Y. (2021) Oral Candidosis: Pathophysiology and Best Practice for Diagnosis, Classification, and Successful Management. *Journal of Fungi,* 7(7),555-563

Mabrouk M., Das D.B., Salem Z.A., Beherei H.H. (2021) Nanomaterials for Biomedical Applications: Production, Characterisations, Recent Trends and Difficulties. *Molecules,* 26(4), 1077-1089

Maitig A.M.A., Alhoot M.A.M., Tiwari K.S. (2018) Isolation and Screening of Extracellular Protease Enzyme from Fungal Isolates of Soil. *Journal of Pure and Applied Microbiology*, 2(4),2059-2067

Mangoyi R., Midiwo J., Mukanganyama S. (2015) Isolation and characterization of an antifungal compound 5-hydroxy-7,4'-dimethoxyflavone from Combretum zeyheri. *BMC Complement Altern Med*, 15,405-418

Manoharan R.K., Lee J.H., Kim Y.G., Lee J. (2017) Alizarin and Chrysazin Inhibit Biofilm and Hyphal Formation by Candida albicans. *Frontiers in cellular and infection microbiology*, 7,447-459

Maubon D., Garnaud C., Calandra T., Sanglard D., Cornet M. (2014) Resistance of Candida spp. to antifungal drugs in the ICU: where are we now? Intensive *Care Med*, 40(9),1241-55

Mayer F.L., Wilson D., Hube B. (2013) Candida albicans pathogenicity mechanisms. *Virulence,* 4(2),119-28

McCord J.M., Fridovich I. (1969) The utility of superoxide dismutase in studying free radical reactions. I. Radicals generated by the interaction of sulfite, dimethyl sulfoxide, and oxygen. *J Biol Chem*, 244(22),6056-63

Mech F., Wilson D., Lehnert T., Hube B., Thilo Figge M. (2014) Epithelial invasion outcompetes hypha development during Candida albicans infection as revealed by an image-based systems biology approach. *Cytometry Part A*, 85(2),126-139

Miao Y., Tenor J.L., Toffaletti D.L., et al. (2016) Structures of trehalose-6-phosphate phosphatase from pathogenic fungi reveal the mechanisms of substrate recognition and catalysis. *Proc Natl Acad Sci U S A,* 113(26),7148-53

Mohandas J., Marshall J.J., Duggin G.G., Horvath J.S., Tiller D.J. (1984) Differential distribution of glutathione and glutathione-related enzymes in rabbit kidney. Possible implications in analgesic nephropathy. *Biochem Pharmacol,* 33(11),1801-7

Mohesien, M., Moussa, H., Serag, M., Adel El-Gendy, M., El-Zahed, M. (2023). Mycogenical Synthesising AgNPs Using Two Native Egyptian Endophytic Fungi Isolated from Poisonous Plants. Egyptian Journal of Botany, 63(2), 403-417. doi: 10.21608/ejbo.2022.167290.2160

Müller C.A., Obermeier M.M., Berg G. (2016) Bioprospecting plant-associated microbiomes. *Journal of biotechnology*, 235,171-80

Murray P.R., Baron E.J., Pfaller M.A., Tenover F.C., Yolke R.H. (1995) Manual of Clinical Microbiology, 6th edn. ASM Press

Netala V.R., Kotakadi V.S., Bobbu P., Gaddam S.A., Tartte V. (2016) Endophytic fungal isolate mediated biosynthesis of silver nanoparticles and their free radical scavenging activity and anti microbial studies. *3 Biotech*, 6(2),132-145

Othman A., Elsayed M., Elshafei A., Hassan M. M. (2016) Nano-silver biosynthesis using culture supernatant of Penicillium politans NRC510: Optimization, characterization and its antimicrobial activity. *International Journal of ChemTech Research,* 9,433-444

Pande M., Dubey V.K., Yadav S.C., Jagannadham M.V. (2006) A novel serine protease cryptolepain from Cryptolepis buchanani: purification and biochemical characterization. *J Agric Food Chem,* 54(26),10141-50

Patra J.K., Baek K.H. (2017) Antibacterial Activity and Synergistic Antibacterial Potential of Biosynthesized Silver Nanoparticles against Foodborne Pathogenic Bacteria along with its Anticandidal and Antioxidant Effects. *Frontiers in microbiology*, 8,167-179

Pradhan S., Roy G.S. (2013) Study the Crystal Structure and Phase Transition of BaTiO 3 - A Pervoskite. In,.

Radhakrishnan V.S., Reddy Mudiam M.K., Kumar M., Dwivedi S.P., Singh S.P., Prasad T. (2018) Silver nanoparticles induced alterations in multiple cellular targets, which are critical for drug susceptibilities and pathogenicity in fungal pathogen (Candida albicans). *International journal of nanomedicine,* 13,2647-2663

Rahimi-Nasrabadi M., Pourmortazavi S.M., Shandiz S..A, Ahmadi F., Batooli H. (2014) Green synthesis of silver nanoparticles using Eucalyptus leucoxylon leaves extract and evaluating the antioxidant activities of extract. *Nat Prod Res*, 28(22),1964-9

Rajendran R., Sherry L., Nile C.J., et al. (2016) Biofilm formation is a risk factor for mortality in patients with Candida albicans bloodstream infection-Scotland, 2012-2013. *Clin Microbiol Infect,* 22(1),87-93

Ribeiro L.G., Roque G.S.C., Conrado R., De Souza A.O. (2023) Antifungal Activity of Mycogenic Silver Nanoparticles on Clinical Yeasts and Phytopathogens. *Antibiotics (Basel)*, 12(1),91-103

Różalska B., Budzyńska A., Micota B., Sadowska B. (2014) New strategies to combat biofilm-associated infections. Part I. The therapeutic potential of antimicrobial peptides. In,

Różalska B., Sadowska B., Budzyńska A., Bernat P., Różalska S. (2018) Biogenic nanosilver synthesized in Metarhizium robertsii waste mycelium extract - As a modulator of Candida albicans morphogenesis, membrane lipidome and biofilm. *PloS one,* 13(3):e0194254

Şanlı K., Arslantaş E., Ceylan A.N., Öncel B., Özkorucu D., Özkan Karagenç A. (2024) Candidemia in Pediatric-Clinic: Frequency of Occurrence, Candida Species, Antifungal Susceptibilities, and Effects on Mortality (2020-2024). *Diagnostics (Basel, Switzerland),* 14(20),2343-54

Santana I.L., Gonçalves L.M., de Vasconcellos A.A., da Silva W.J., Cury J.A., Del Bel Cury A.A. (2013) Dietary carbohydrates modulate Candida albicans biofilm development on the denture surface. *PloS one,* 8(5):e64645

Singh H., Desimone M.F., Pandya S., et al. (2023) Revisiting the Green Synthesis of Nanoparticles: Uncovering Influences of Plant Extracts as Reducing Agents for Enhanced Synthesis Efficiency and Its Biomedical Applications. *International journal of nanomedicine,* 18,4727-4750

Sun L., Liao K., Li Y., et al. (2016) Synergy Between Polyvinylpyrrolidone-Coated Silver Nanoparticles and Azole Antifungal Against Drug-Resistant Candida albicans. *Journal of nanoscience and nanotechnology,* 16(3),2325-2335

Teranishi Y., Tanaka A., Osumi M., Fukui S. (1974) Catalase Activities of Hydrocarbon-utilizing Candida Yeasts. *Agricultural and biological chemistry,* 38,1213-1220

Vazquez-Muñoz R., Avalos-Borja M., Castro-Longoria E. (2014) Ultrastructural analysis of Candida albicans when exposed to silver nanoparticles. *PloS one*, 9(10),e108876

Villar C.C., Kashleva H., Nobile C.J., Mitchell A.P., Dongari-Bagtzoglou A. (2007) Mucosal tissue invasion by Candida albicans is associated with E-cadherin degradation, mediated by transcription factor Rim101p and protease Sap5p. *Infection and immunity*, 75(5),2126-35

Waksman S.A. (1922) A Method for Counting the Number of Fungi in the Soil. *J Bacteriol,* 7(3),339-41

Wang D., Xue B., Wang L., Zhang Y., Liu L., Zhou Y. (2021) Fungus-mediated green synthesis of nano-silver using Aspergillus sydowii and its antifungal/antiproliferative activities. *Scientific Reports,* 11(1),10356-68

Zaheer N., Tewari KK, Krishnan PS (1967) Mitochondrial forms of glucose 6-phosphate dehydrogenase and 6-phosphogluconic acid dehydrogenase in rat liver. *Archives of biochemistry and biophysics,* 120(1),22-34

Zwar I.P., Trotta C.D.V., Ziotti A.B.S., et al. (2023) Biosynthesis of silver nanoparticles using actinomycetes, phytotoxicity on rice seeds, and potential application in the biocontrol of phytopathogens. *J Basic Microbiol.* 63(1),64-74.

Supplementary Figure. *Aspergillus* and *Penicillium* were signified by more than three species among the isolates.

Supplementary Table. Isolation, colonialization, and dominance frequency of fungi isolated from the rhizosphere of *Reseda pentagyna*.

Fungal species					
Genus	**Species**	**Isolate code**	**No.**	**% CF**	**% DF**
			55		
Aspergillus	*A. flavus*	F1	15	5.6	10
	A. terreus	F2	9	3.7	7.1
	A. oryzae	F3	6	3.3	6.1
	A. parasiticus	F4	22	6.1	12.2
	A. nomius	F-5	4	1	2
			40		
Penicillium	*P. oxalicum*	F6	6	3.3	6.2
	P. griseofulvum	F7	21	7	13.2
	P. fellutanum	F8	9	3.9	6
	P. citrinum	F9	3	0.8	1.4
			5		
Alternaria	*A. alternate*	F10	2	1	2
	A. tenuissima	F11	3	2	3.9
			17		
Rhizopus	*R. oryzae*	F12	13	2	3.9
	R. stolonifer	F13	4	4	8
			38		
Fusarium	*F. oxysporum*	F14	25	6	12